Breaking the diffraction barrier outside of the optical near-field with bright, collimated light from nanometric apertures

Peter R. H. Stark*†, Allison E. Halleck*, and Dale N. Larson‡

*Department of Biochemistry and Molecular Pharmacology and ‡Technology Engineering Center, Harvard Medical School, Boston, MA 02115

Communicated by David E. Clapham, Harvard Medical School, Boston, MA, October 11, 2007 (received for review May 23, 2007)

The optical diffraction limit has been the dominant barrier to achieving higher optical resolution in the fields of microscopy, photolithography, and optical data storage. We present here an approach toward imaging below the diffraction barrier. Through the exposure of photosensitive films placed a finite and known distance away from nanoscale, zero-mode apertures in thin metallic films, we show convincing, physical evidence that the propagating component of light emerging from these apertures shows a very strong degree of collimation well past the maximum extent of the near-field ($\lambda_0/4n$–$\lambda_0/2n$). Up to at least 2.5 wavelengths away from the apertures, the transmitted light exhibits subdiffraction limit irradiance patterns. These unexpected results are not explained by standard diffraction theory or nanohole-based "beaming" rationalizations. This method overcomes the diffraction barrier and makes super-resolution fluorescence imaging practical.

fluorescence microscopy | nanoholes | subdiffraction limit | subwavelength imaging | super-resolution

The spatial resolution of an optical system operating outside of the optical near-field can given by the Rayleigh criterion (1),

$$W = 0.61\lambda/NA, \qquad [1]$$

where λ is the wavelength of the emitted photons and NA is the numerical aperture of the system. This criterion says that two point sources can be "just resolved" when their separation is W. The 0.61 term arises from the superposition of two Fraunhofer diffraction patterns for circular apertures (Airy disks) such that the principle maximum of one of the patterns coincides with the first minimum of the other. This superposition of two sources at distance W results in an intensity distribution of two peaks with a valley between with a contrast ratio (ratio of peak to valley intensities) of 0.81.

In an effort to circumvent this limit, a method was first proposed in which light is leaked through an aperture much smaller than the wavelength in an opaque screen (2). Because the light through such an aperture is known to diffract heavily and the power flux through such an aperture is evanescent, the aperture must be placed in the optical near-field of the probe. This method, practically realized, is called near-field scanning optical microscopy (NSOM) (3–5). Super-resolution (resolution values smaller than W, above) with NSOM has been demonstrated often. NSOM, however, suffers from the low photon flux through a zero-mode waveguide (6, 7) and the requirement of strict maintenance of surface-to-aperture distance within a few nanometers (8). Parallel probe NSOM approaches have been proposed and developed in which a plate with periodic perforations of zero-mode waveguides is placed on top of a sample in the optical near-field (9, 10).

The behavior of light emitted from periodically perforated arrays of subwavelength apertures in metal films on mesoscopic length scales, between the length regime where light classically propagates ($d \gg \lambda$; the far-field) and the range where it displays evanescent properties (shorter than half of a wavelength; the near-field), is poorly understood. Studies and numerical simulations in the near-field are an active area of investigation (11–13). Far-field numerical simulations and measurements of light through these nanoholes have been accomplished in numerous investigations (13–20). Some data about the meso-field (between far-field and near-field) can be deduced from both sets of studies. However, there exist very few data specific to the meso-field, and resolution in this regime is limited. Janssen *et al.* (21) explored this region in numerical modeling of multiple slits in metals. It is often recognized that slit arrays, although they can provide some insight into the phenomenon of extraordinary optical transmission (EOT) in hole arrays, cannot sufficiently explain it because slits can support transverse electric and magnetic (TEM) modes; and, therefore, the transmission properties of slit arrays in metal will most likely be different from those in hole arrays in the same metal (20, 22). To gain experimental access to this poorly understood length regime, we fabricated two classes of test structures constructed of optically thick metallic films deposited on substrates or superstrates. The metallic layers were periodically perforated with nominally cylindrical apertures by a focused ion beam instrument (23).The perforation period, a_0, was chosen to excite surface plasmon (SP)/photon coupling via grating momentum on an otherwise smooth surface (24). It was expected that extraordinary optical transmission (25) through arrayed nanoholes and beaming phenomenon (26) would allow significantly higher signal-to-noise ratios in the collection process. The structures were exposed to monochromatic, constant irradiance light, and images were recorded in different media.

Results and Discussion

Initial experiments were conducted with hexagonally arranged aperture lattices of diameter $\phi = 150$ nm in 100 nm Au on a 4-nm adhesion layer of Cr on borosilicate glass (Fig. 1, first class of structure). Collimated, unpolarized narrow-band light (4 nm FWHM) was directed at 90° onto the Au–air interface, and the light emergent from the Au-Cr–glass interface was collected in the far-field via a conventional microscope and CCD. Collected images show 1:1 correlation from the emission sites on the backside (nonilluminated side) to the apertures. The lattice constant and aperture size were conserved in the image. Scattering of light emerging from the apertures and the radiative decay of the SP on the back side [whose interference is widely accepted to be the cause of beaming (17, 26, 27)] were not detected, even when the focal plane of the lens was placed on the

Author contributions: P.R.H.S. and A.E.H. contributed equally to this work; P.R.H.S. designed research; P.R.H.S. and A.E.H. performed research; D.N.L. contributed new reagents/analytic tools; P.R.H.S. and A.E.H. analyzed data; and P.R.H.S. wrote the paper.

The authors declare no conflict of interest.

†To whom correspondence should be addressed. E-mail: peter_stark@hms.harvard.edu.

www.pnas.org/cgi/doi/10.1073/pnas.0709701104

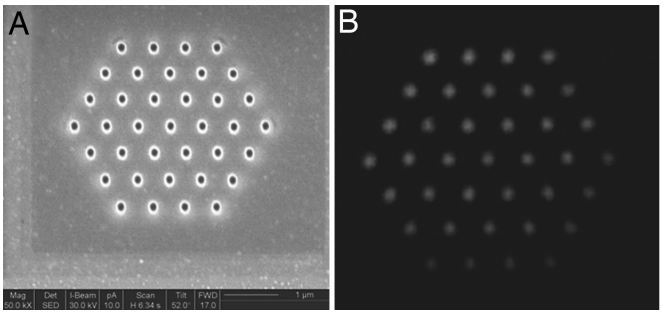

Fig. 1. Far-field transmission of light through subwavelength apertures in a metal film. (*A*) Focused ion beam image of gold–air interface of hexagonal aperture array in a composite metal film on an insulator (100 nm Au on 4 nm Cr on borosilicate cover glass). The aperture, ϕ, is 150 nm in diameter with lattice constant $a_0 = 500$ nm. (*B*) Image taken of the emission from the device through the borosilicate on an inverted microscope with illumination on the Au side. The image was collected at ×100/1.4 N.A. with 550-nm nonpolarized, normal illumination on the gold–air interface. The decrease in observed power at the bottom is due to inconstant irradiance.

emission surface of the metal. This result was unexpected and contrary to earlier predictions. In a somewhat similar experiment completed by Docter *et al.* (28), images of a rectangular hole array were captured while varying numerical aperture of the collection lens. Their results also show 1:1 correlation and no, or very little, photonic information between the holes. Their arrays, although, differ from that shown if Fig. 1 in that, at the given numerical apertures and wavelength of the illuminating light, the direct transmission from the holes should be resolvable according the Rayleigh criterion. Scattering and radiative decay components were expected to show quite large power densities well into the far-field, with a lateral extent much larger than the period of the apertures resulting in overlapping and strong interference patterns. However, the images were well defined and showed minimal interference or diffractive effects.

The second structure (Fig. 2) was designed to probe the meso-field and edge of the near-field. In contrast to the first experiment, the light source was a solid-state laser ($\lambda_0 = 410$ nm)

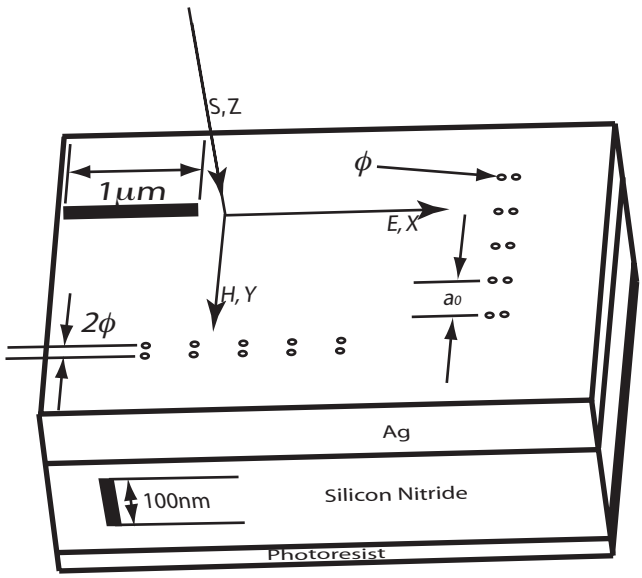

Fig. 2. Schematic cross-section of test structure used for determination of photon properties in meso-field. The aperture size, ϕ, is 60 nm, $a_0 = 393$ nm, The "TE array" is on the right. The "TM array" is at the bottom. The polarization ratio is >1,000:1.

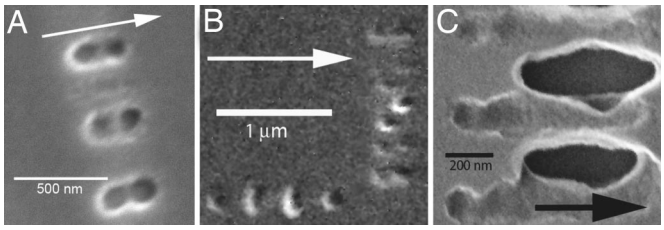

Fig. 3. Direct-write patterning of photoresist at 0.5λ distance. (*A*) Scanning electron micrograph, at ×150,000, of twinned holes in patterned photoresist at λ/2 (100 nm) distance from the 60-nm apertures spaced at 120 nm apart in the Ag film. The direction of the incident polarization is indicated by the arrow. (*B*) SEM image, at ×35,000, of twinned holes in photoresist at λ (200 nm) distance from the apertures. (*C*) SEM image, at ×150,000, of twinned holes in photoresist at 2.5λ (500 nm) distance from the apertures. The twinned holes are on the left. The hole-set to hole-set interference is on the right.

with additional polarization optics to deliver more highly collimated, monochromatic, and strongly polarized light to the metallic film. This second class of structures had smaller (60 nm) apertures in 110-nm layers of Ag sputtered onto membranes of low-stress silicon nitride. The thickness of the silicon nitride membranes was varied from 75 to 500 nm. The period of the perforations was designed to allow coupling of the normally incident photons with SPs at the air–Ag interface. SP can be readily elicited on gratings by transverse magnetic (TM) field light (24) but only weakly by transverse electric (TE) field light (29). With strong coupling of the SP and the TM light, any two-dimensional array should behave as a set of linear arrays when the polarization direction is parallel to the grating vector (the direction defined by a_0). Along the direction normal to the polarization, these sets should be weakly coupled. We milled two orthogonal sets of closely spaced linear arrays in the silver. We call the sets of linear arrays in which the electric field vector is aligned with the grating vector "TM arrays." The orthogonal sets, which we call "TE arrays," should not strongly couple the TM field with SP in the silver film and thus should not show the SP-enhanced transmission expected of the TM arrays. In the TE arrays, the electric field vector is parallel to the separation distance, which was fixed at 2ϕ. This distance was chosen specifically not to satisfy the strong photon/SP coupling condition of the two linear arrays but still remain below the diffraction limit for a perfect lens and, thus, would not be resolvable by a diffraction-limited system (1).

It is important not to distort the local field anisotropically when probing the meso-field, and especially the near-field, of the metallic film because the nanohole arrays show extreme sensitivity to the local dielectric function (30). We chose a photosensitive film placed within the range of interest as a suitable method of image recording. The film must, though, have very small features, such as grain size, roughness, etc., when compared with the typical dimensions of the irradiated area (8, 31). A thinned conventional photoresist was spin-coated on the back side of the silicon nitride membranes. The dielectric spacer layer must be flat. We showed in earlier experiments that depositing spacer layers either by spinning liquids such as poly(methyl methacrylate) (PMMA) or by chemical or physical vapor deposition resulted in coatings that conformed to the surface and were not flat. Even with no radiative exposure, photoresist spun onto a conformal spacer layer is also conformal. Regardless of the tone (positive or negative) of the photoresist, a conformal coating results in an anisotropic field in the near-field of the apertures, distorting the measurement (32). The direct application of the photoresist to the silicon nitride also excludes any intermediate materials, which would vastly complicate the interpretations of the results. Our method (a solid, flat dielectric

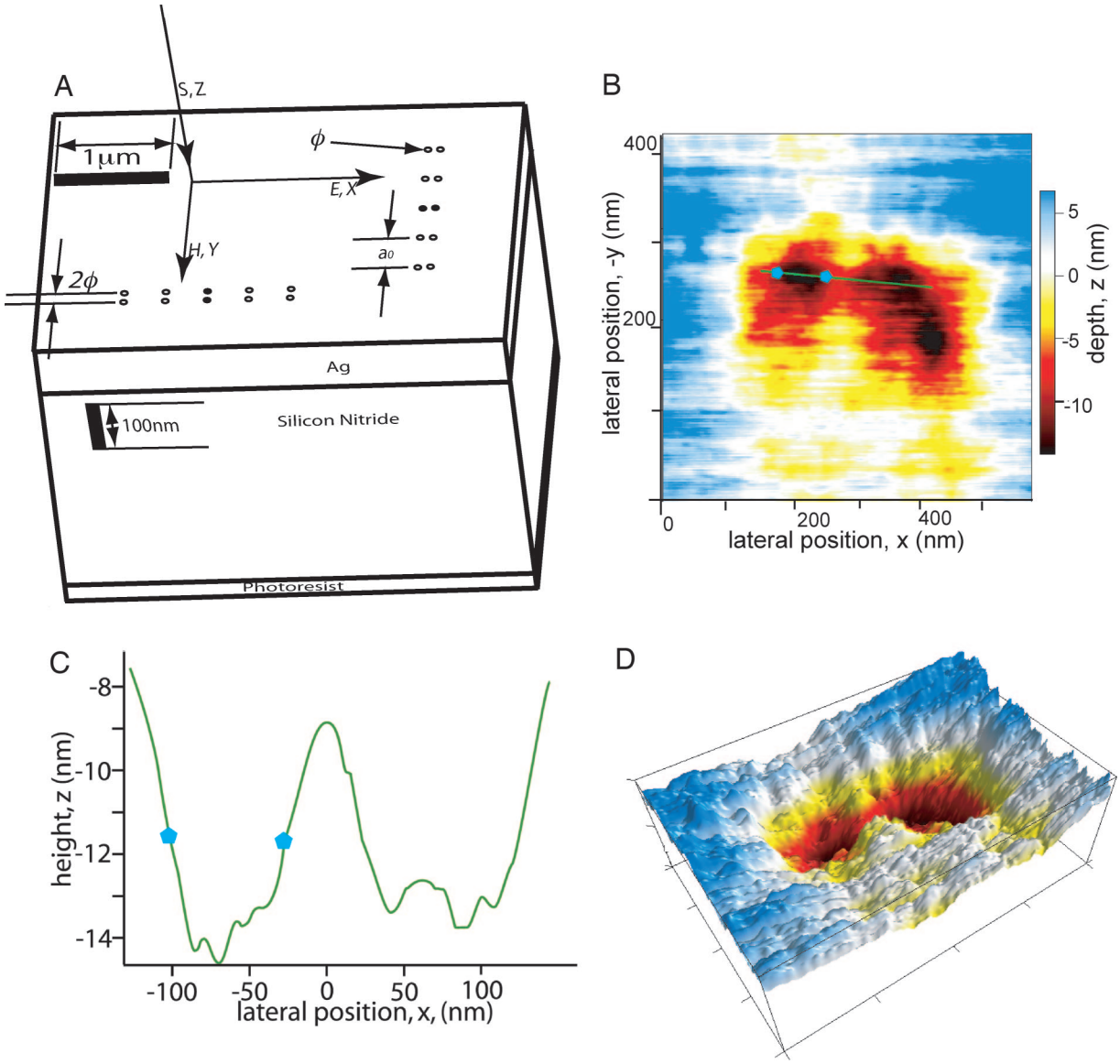

Fig. 4. Direct-write patterning of photoresist at 2.5λ distance. (*A*) Schematic cross-section of test structure used for determination of photon properties in meso-field. This structure eliminates the hole-set to hole-set interference seen in the test structure portrayed in Fig. 2. The twinned holes (shown as filled circles) and dimples (indicated as open circles), both ϕ = 60 nm in diameter, are spaced apart by twice their diameter in one dimension and by A_0 = 393 nm in the orthogonal dimension. The depth of the dimples is 30 nm. (*B*) Patterning of features below the diffraction limit and well outside of the optical near-field. The AFM images and section of the image of patterned photoresist at a working distance of 2.5λ show direct patterning via TE nanometric aperture/corrugation (ϕ = 60 nm) arrays in Ag film. The depth of features is indicated by the linear scale bar on the right side of the figure. The green line in the view, punctuated by pink pentagons, is shown in an orthogonal view in *C*. (*D*) Three-dimensional view of the same area. The contrast of the exposed and developed photoresist in relation to the unexposed resist remaining between the two holes clearly is better than should be expected from the diffraction limit.

spacer layer with Ag sputtered on one side and photoresist spin-coated on the other) was chosen to record the irradiance produced by the nanohole array at the distance determined by the thickness of the silicon nitride membrane while satisfying the requirements of the relative isotropy compared with the size of the irradiance patterns and the wavelength of the incident light.

The silver side of the laminates was exposed to various doses of well defined pulse widths of laser light (λ_0 = 410 nm). After exposure, the structures were immersed in diluted developer and then in water to stop and fix the development process. The fully processed structures were analyzed both by atomic force microscopy (AFM) and scanning electron microscopy (SEM). Parallel membranes were fabricated for each dose of laser light, one to be imaged by AFM the other by SEM, because even fixed photoresist films lose contrast when exposed to high-energy electrons.

TE arrays on the silicon nitride spacers, which ranged in thickness from ≈λ/2.7 (75 nm) to 2.5λ (500 nm), show high-contrast patterning of the photoresist. (λ_0 = 410 nm. In the silicon nitride of n = 2.02, λ = 203 nm.) The twinned holes are quite apparent in low-power (<5 keV) SEM images (Fig. 3*A* and *B*). At λ/2 distances, interference between the twinned hole-sets begins to appear (Fig. 3*B*). The patterning of the double holes relative to this interference decreases with increasing distance. At a 2.5λ (500 nm) distance from the apertures, the interference dominates, and the twinned holes are barely discernible (Fig. 3*C*). The hole-set to hole-set interference was eliminated in another 2.5λ sample by using a scheme in which resonant

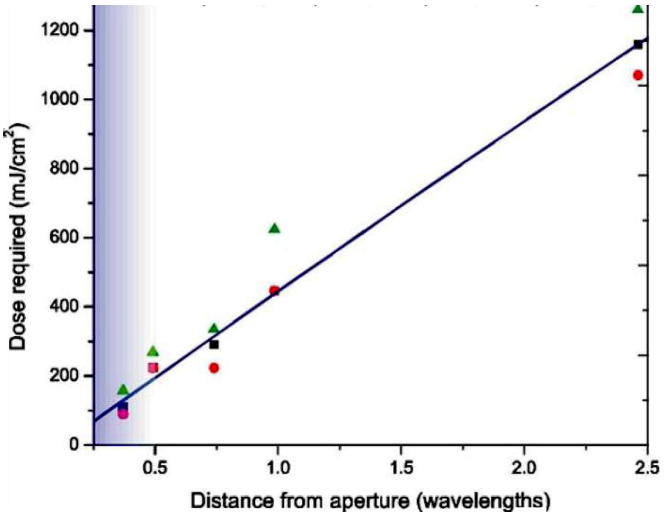

Fig. 5. Required dose for production of twinned holes in TE arrays versus working distance. The subjectivity of estimation of contrast requires bracketing. The minimum dose required for sufficiently good contrast in multiple samples is indicated by the filled circles. Doses larger than those indicated by the triangles resulted in poor contrast between holes. Optimum patterning is marked by the squares. The squares appear to define a linear dose–response relationship. The blue gradient on the left side of the chart indicates optical power in the near-field of the metal film.

electromagnetic surface waves are excited by periodic surface features that do not penetrate the metallic film (16, 33). These features flank the single holes and still maintain the TE orientation (Fig. 4*A*). This method provides the same excitement as seen in the paired TE arrays but allows transmission only through one pair of holes. The patterning of the photoresist by the twinned holes is readily perceived in the AFM images (Fig. 4 *B* and *C*). TM arrays, on the other hand, poorly reproduced the twinned holes, producing oval exposed areas. TM arrays, in addition, did not show noticeably increased power transmission over the TE cases. Multiple experiments were completed for each distance to bracket the exposure dose required to produce the highest contrast. For an evanescent field, an exponential increase in required dose vs. distance from apertures is expected. For point sources, the dose is expected to follow a distance-squared relationship. However, the dose–distance relationship observed was linear (Fig. 5). This linear dependence suggests that the source was highly collimated in one direction, with linear divergence in another. This conclusion is substantiated by the lack of contrast apparent in the twinned holes in the TM arrays when compared with the TE arrays. For the TE arrays, in which the twinned holes are readily apparent, the divergence in the direction of the magnetic field is small, and the divergence in the direction of the electric field is minimal.

Because of the nonlinearity of contrast produced in photoresist as a function of dose, very small isolated features can be made through underdevelopment of the irradiated area, effectively sampling only the very center of that area. These isolated features can be mistaken for subdiffraction-sized irradiance patterns. Creating two very closely spaced features in photoresist, however, is subject to the Rayleigh criterion for point sources. For a lensed system imaging a periodic grating outside of the near-field, this follows $P_{min}(\lambda, N) = \lambda/N$ (34). Below this minimum separation, $P_{min}(410\text{ nm}, 2.02) = 203$ nm, there should be very little difference in the irradiance levels between the geometric axes of the sources and their centers, thus leaving very little perceivable contrast in the image in the developed photoresist. Regardless of development conditions, a positive feature between two holes in the photoresist indicating two separate sources of irradiance would not be predicted. In the near-field, where the power is evanescent and decays exponentially, this is not the case (8), and feature separation smaller than that dictated by the Rayleigh criterion can be created. Indeed, the currently published numerical simulations involving many different methods all show that any subdiffraction-limited information is not transmitted beyond the near-field (13, 15, 16, 27, 35, 36). For "beaming" from single apertures, models suggest that the effect is the product of emission from the surface of the metal film. When beaming and the associated focusing occurs, there should be no information below the diffraction limit available in either near-field or far-field (13, 27, 35). In the case of multiple apertures, simulations predict that emissions from the apertures and the metal surfaces interfere, resulting in patterns similar to those from gratings, and that there is not one-to-one registration of apertures to principle spots of irradiance produced beyond the near-field (36).

Conclusion

In summary, we have demonstrated anomalous behavior of photons in the meso-field. Here, photons can display a semicollimated behavior well outside of the optical near-field, while irradiating areas of dimensions substantially smaller than the diffraction limit for light. In this domain, photons do not display the properties associated with evanescent fields, as would be expected from standard diffraction theory. Given that the near-field's maximum decay length is ≈100 nm in this medium, the results would be expected to adhere to a model of a collection of point sources on the emission plane and behave as a miniature phased array antenna. However, the results are not explained by near-field or far-field theory and numerical models, and thus require more understanding of the behavior of light in the meso-domain. Regardless of the mechanism, our technique may find immediate application in super-resolution including data storage and retrieval, super-resolution fluorescence and bright-field microscopy, and photolithography.

Materials and Methods

In the first class of structure, propagating meso-field (due to the finite depth of focus) and far-field information was collected on a CCD camera (AxioCam; Zeiss MicroImaging) through the intermediate optics of a ×100/1.4-N.A. oil immersion objective-equipped inverted microscope (Nikon). The depth of focus of this lens is ≈495 nm at this wavelength. Monochromatic light (2 nm FWHM) from a focused white light source (Xe arc) was delivered to the structure through a double monochromator (Instruments S.A./Jobin Yvon). It was found that convection currents in the bulb envelope lead to inconstant irradiance on the sample. Although we tried different homogenization techniques (diffuser and tunnel homogenizer), we concluded that increased distribution of in-plane momentum of the photons resulted in poorer performance and less sharp images.

For structures on silicon nitride, silver was sputtered to a thickness of 110 nm onto commercially prepared silicon nitride membranes (Silson). A home-built sputter machine was used. Thermal evaporation of the metals was also investigated, but, in the case of the silver, the coatings were found to be unsuitably rough. A conventional G-line photoresist (MicroChem Rohm and Haas S1805) was thinned 2:1 thinner:resist and spin-coated at 6,000 rpm for 45 sec. Because at these concentrations the resist is not easily or permanently suspended in the thinner, the mixture was gently and continuously stirred for a minimum of 24 h before application. The resist then was baked for 60 sec at 105°C. After exposure, the resist-coated membranes were immersed in thinned developer (two parts water to one part developer) for 5 sec.

In both cases, apertures were milled into the metal via focused 30-kV Ga ions (FEI DB235) at 10 pA. Milling rates and depths

were determined through cross-sectioning and destructive examination of several similar samples. The lattice constant, given previously as a_0, was determined for the resonant excitation of surface plasmons via grating/crystal momentum with normal photons according to the equation

$$\lambda_{res} = \frac{a_0}{\nu}\sqrt{\frac{\varepsilon_1\varepsilon_2}{\varepsilon_1 + \varepsilon_2}}, \quad [2]$$

in which λ_{res} is the wavelength of resonance, a_0 is the lattice constant, ν is an integer describing the grating order, ε_1 is the complex dielectric function of the metal, and ε_2 is the dielectric function of the material through which the photons travel before being incident on the metal–dielectric interface. It is important to note that the dielectric functions of the materials not only are spectrally dependent but, especially in thin films, also are heavily dependent on the coating method and conditions (24). In the region of interest, we used high-order Chebyshev polynomials to fit data taken specifically in surface plasmon resonance measurements in which thin films were deposited in similar fashions and conditions to those described above (24, 30). The predictions of our final equations differ somewhat from those found in the literature for surface plasmon resonance measurements because of the doping of the surface close to the apertures by Ga ion overspray and embedment.

AFM data were taken with three different machines. Images presented in this manuscript used an Asylum Research MFP-3D with ultrafine contact-tipped cantilevers of tip diameters <10 nm (MikroMasch). Thickness measurements of the metal coatings were verified by using cross-sectioned scanning electron microscopy: Asylum Research, Park Systems, and Digital Instruments NanoScope IIIa (Veeco Instruments) atomic force microscopes and a Veeco Instruments NT1100 optical profilometer.

We thank W. Bender, D. Clapham, M. Loncar, and A. van Oijen for reading and commenting on the manuscript and T. W. Ebbesen and M. Totzeck for experiment guidance. Much of the basis of this work was performed on equipment donated by D. Clapham. This work was supported by National Institutes of Health/National Cancer Institute Grant 148171.

1. Born M, Wolf E (1980) *Principles of Optics* (Cambridge Univ Press, Cambridge, UK).
2. Synge EH (1928) *Philos Mag* 6:356–362.
3. Pohl D, Denk W, Lanz M (1984) *Appl Phys Lett* 44:651–653.
4. Durig U, Pohl DW, Rohner F (1986) *J Appl Phys* 59:3318–3327.
5. Betzig E, Trautman JK, Harris TD, Weiner JS, Kostelak RL (1991) *Science* 251:1468–1470.
6. Bethe HA (1944) *Phys Rev* 66:163–182.
7. Bouwkamp CJ (1954) *Diffraction Theory* (Physical Society, London).
8. Betzig E, Trautman JK (1992) *Science* 257:189–195.
9. Semin DJ, Ambrose WP, Goodwin PM, Wendt JR, Keller RA (1997) *Proc SPIE* 3009:109–118.
10. Sandoz P, Giust R, Tribillon G (1999) *Opt Commun* 161:197–202.
11. Popov E, Neviere M, Wenger J, Lenne PF, Rigneault H, Chaumet P, Bonod N, Dintinger J, Ebbesen T (2006) *J Opt Soc Am A* 23:2342–2348.
12. Popov E, Neviere M, Boyer P, Bonod N (2005) *Opt Commun* 255:338–348.
13. Egorov D, Dennis BS, Blumberg G, Haftel MI (2004) *Phys Rev B* 70:033404.
14. Degiron A, Ebbesen TW (2004) *Opt Express* 12:3694–3700.
15. Lezec HJ, Thio T (2004) *Opt Express* 12:3629–3651.
16. Lockyear MJ, Hibbins AP, Sambles JR, Lawrence CR (2004) *Appl Phys Lett* 84:2040–2042.
17. Martin-Moreno L, Garcia-Vidal FJ, Lezec HJ, Degiron A, Ebbesen TW (2003) *Phys Rev Lett* 90:167401.
18. Martín-Moreno L, García-Vidal FJ, Lezec HJ, Pellerin KM, Thio T (2001) *Phys Rev Lett* 86:1114–1117.
19. Sarychev AK, Podolskiy VA, Dykhne AM, Shalaev VA (2002) *IEEE J Quantum Electron* 38:956–963.
20. Lomakin V, Michielssen E (2005) *Phys Rev B* 71:235117.
21. Janssen OTA, Urbach HP, 't Hooft GW (2006) *Opt Express* 14:11823–11832.
22. Johansen K, Arwin H, Lundstrom I, Liedberg B (2000) *Rev Sci Instrum* 71:3530–3538.
23. Przybilla F, Degiron A, Laluet JY, Genet C, Ebbesen TW (2006) *J Opt A* 8:458–463.
24. Raether H (1988) *Surface Plasmons on Smooth and Rough Surfaces and on Gratings* (Springer, Berlin).
25. Ebbesen TW, Lezec HJ, Ghaemi HF, Thio T, Wolff PA (1998) *Nature* 391:667–669.
26. Lezec HJ, Degiron A, Devaux E, Linke RA, Martin-Moreno L, Garcia-Vidal FJ, Ebbesen TW (2002) *Science* 297:820–822.
27. Garcia-Vidal FJ, Martin-Moreno L, Lezec HJ, Ebbesen TW (2003) *Appl Phys Lett* 83:4500–4502.
28. Docter MW, Young IT, Piciu OM, Bossche A, Alkemade PFA, van den Berg PM, Garini Y (2006) *Proc SPIE* 6195:61951L.
29. Watts RA, Preist TW, Sambles JR (1997) *Phys Rev Lett* 79:3978–3981.
30. Stark PRH, Halleck AE, Larson DN (2005) *Methods* 37:37–47.
31. Srituravanich W, Fang N, Durant S, Ambati M, Sun C, Zhang X (2004) *J Vac Sci Technol B* 22:3475–3478.
32. Girard C, Joachim C, Gauthier S (2000) *Rep Prog Phys* 63:893–938.
33. Thio T, Pellerin KM, Linke RA, Lezec HJ, Ebbesen TW (2001) *Opt Lett* 26:1972–1974.
34. Melville DOS, Blaikie RJ (2005) *Opt Express* 13:2127–2134.
35. Martin-Moreno L, Garcia-Vidal FJ (2004) *Opt Express* 12:3619–3628.
36. Wannemacher R (2001) *Opt Commun* 195:107–118.